Journal of Alloys and Compounds 509 (2011) 5604–5610

Contents lists available at ScienceDirect

Journal of Alloys and Compounds

journal homepage: www.elsevier.com/locate/jallcom

Gaseous and electrochemical hydrogen storage kinetics of nanocrystalline Mg_2Ni-type alloy prepared by rapid quenching

Yang-huan Zhang[a,b,*], Bao-wei Li[a], Hui-ping Ren[a], Feng Hu[a,b], Guo-fang Zhang[a,b], Shi-hai Guo[b]

[a] Elected State Key Laboratory, Inner Mongolia University of Science and Technology, Baotou 014010, China
[b] Department of Functional Material Research, Central Iron and Steel Research Institute, Beijing 100081, China

ARTICLE INFO

Article history:
Received 12 November 2010
Received in revised form 16 February 2011
Accepted 17 February 2011
Available online 23 February 2011

Keywords:
Mg_2Ni-type alloy
Rapid quenching
Substituting Ni with Cu
Hydrogen storage kinetics

ABSTRACT

The nanocrystalline Mg_2Ni-type $Mg_2Ni_{1-x}Cu_x$ (x = 0, 0.1, 0.2, 0.3, 0.4) alloys were synthesized by direct melt quenching technique. The structures of the as-cast and quenched alloys were investigated by XRD, SEM and HRTEM. The gaseous hydrogen storage kinetics of the alloys was measured using an automatically controlled Sieverts apparatus. The electrochemical hydrogen storage kinetics of the alloys was tested by using constant current to charge and discharge the electrode. The results indicate that the substitution of Cu notably rendered the grain refinement of the as-cast alloys without altering the major phase Mg_2Ni. All the as-quenched alloys exhibit a nanocrystalline structure without the presence of any amorphous phase. It is found that the substitution of Cu for Ni and rapid quenching significantly ameliorated the gaseous and electrochemical hydrogen storage kinetics of the nanocrystalline $Mg_2Ni_{1-x}Cu_x$ (x = 0–0.4) alloys. Furthermore, both the rapid quenching treatment and the Cu substitution results in a notable increase in the hydrogen diffusion coefficient (D) as well as the limiting current density (I_L) but an obvious decline in the electrochemical impedance.

1. Introduction

Mg_2Ni-type intermetallic compounds are the most promising materials for hydrogen storage [1] and Ni-MH batteries [2] owing to their abundance, light weight, and high hydrogen capacity, e.g. 3.6 wt.% for Mg_2NiH_4, 4.5 wt.% for Mg_2CoH_5 and 5.4 wt.% for Mg_2FeH_6. However, their practical application to hydrogen suppliers has been limited mainly due to their sluggish hydriding/dehydriding kinetics as well as high thermodynamic stability of their corresponding hydride. It has already been documented that the significant developments have been made in ameliorating the hydrogen absorption/desorption kinetics of the Mg-based alloys. However, the key challenge about the reduction in thermodynamic stability of Mg based hydrides still remains intact.

The hydrogen storage kinetics of the Mg-based alloy is strongly dependent upon the nature of its alloying elements and structure. It is reported that the use of various non-equilibrium processing techniques such as mechanical alloying (MA) [3,4] and melt quenching [5] has improved the hydrogen absorption and desorption kinetics of Mg and Mg-based alloys by virtue of the formation of a nanocrystalline or nano-amorphous structure. As reported by Wu et al. [6], the kinetics of the hydrogen absorption/desorption reactions of the melt-spun Mg–10Ni–2Mm (at.%) alloy ribbons was greatly improved by increasing the quenching rate, and a maximum hydrogen storage capacity of 5.1 wt.% H was obtained. Kalinichenka et al. [7] testified that Mg–Cu–Ni–Y system alloys, prepared by melt spinning technology, can reach reversible gravimetric hydrogen storage densities of up to 4.8 wt.% H_2. Even at a low temperature of 100 °C, the hydrogenation kinetics of the investigated alloys is rather high in the range of 1.5 wt.% H_2 per hour. Révész et al. [8] found that the maximum absorption capacity of ball-milled nanocrystalline $Mg_{70}Ni_{30}$ powder, which was subjected to heavy shear deformation by the process of high-pressure torsion (HPT), is increased by 30–50%. Lang et al. [9] also reported that severe plastic deformation performed by a vertical cold rolling apparatus could be used to enhance hydrogen sorption properties of metal hydrides. The hydrogen sorption kinetics of magnesium hydride, after only five rolling passes, was greatly enhanced without noticeable loss of capacity.

Our previous work has testified that the substitution of Co for Ni and the melt spinning process significantly ameliorated the hydriding and dehydriding kinetics of the Mg_2Ni-type alloys [10,11]. Therefore, it is highly desirable to investigate the influence of substituting Ni with Cu on the hydrogen storage kinetics of Mg_2Ni-type alloys. The Mg_2Ni-type $Mg_2Ni_{1-x}Cu_x$ (x = 0–0.4) alloys have been synthesized by rapid quenching technology. Furthermore, the

* Corresponding author at: Department of Functional Material Research, Central Iron and Steel Research Institute, 76 Xueyuan Nan Road, Haidian District, 100081 Beijing, PR China. Tel.: +86 010 62187570; fax: +86 010 62183115.
E-mail address: zyh59@yahoo.com.cn (Y.-h. Zhang).

0925-8388/$ – see front matter © 2011 Elsevier B.V. All rights reserved.
doi:10.1016/j.jallcom.2011.02.085

effects of both the rapid quenching and the Cu substitution on the structures and the gaseous as well as the electrochemical hydrogen storage kinetics of the alloys have been investigated in detail.

2. Experimental

The nominal compositions of the experimental alloys were $Mg_2Ni_{1-x}Cu_x$ ($x = 0$, 0.1, 0.2, 0.3, 0.4). For convenience, the alloys were denoted with Cu content as Cu_0, $Cu_{0.1}$, $Cu_{0.2}$, $Cu_{0.3}$ and $Cu_{0.4}$, respectively. The experimental alloys were prepared by using a vacuum induction furnace in a helium atmosphere at a pressure of 0.04 MPa. A part of the as-cast alloys was re-melted and quenched by rapid quenching with a rotating copper roller cooled by water. The quenching rate was approximately expressed by the linear velocity of the copper roller. The quenching rates, used in the experiment, were15, 20, 25 and 30 m/s, respectively.

A Philips SEM (QUANTA 400) linked with an energy dispersive spectrometer (EDS) was used for morphological characterization and chemical analysis of the as-cast alloys.

The phase structures of the as-cast and quenched alloys were determined by X-ray diffraction (XRD) (D/max/2400). The diffraction, with the experimental parameters of 160 mA, 40 kV and 10°/min respectively, was performed with $CuK_{\alpha 1}$ radiation filtered by graphite. The effective grain sizes were calculated from Scherrer's formula [12].

The thin film samples of the as-quenched alloys were prepared by ion etching method in order to observe the morphology with high resolution transmission electron microscope (HRTEM) (JEM-2100F, operated at 200 kV), and also to determine the crystalline state of the samples with electron diffraction (ED). The average grain sizes of the as-quenched alloys were measured by a linear intercept method on the HRTEM micrographs.

The gaseous hydrogen absorption and desorption kinetics of the alloys were measured by an automatically controlled Sieverts apparatus. Prior to measuring the hydriding and dehydriding kinetics of the alloys, several hydrogen absorbing and desorbing cycles were performed in order to activate the materials. The hydrogen absorption was conducted at 1.5 MPa and 200 °C, and the hydrogen desorption was carried out at a pressure of 1×10^{-4} MPa and 200 °C, too.

The alloy ribbons were pulverized into fine powder of about 20 μm by mechanical milling and then mixed with carbonyl nickel powder in a weight ratio of 1:4. The mixture was cold pressed under a pressure of 35 MPa into round electrode pellets of 10 mm in diameter and total mass of about 1 g. The electrochemical hydrogen storage kinetics of the alloy electrodes were tested by a tri-electrode open cell, consisting of a metal hydride electrode, a sintered $NiOOH/Ni(OH)_2$ counter electrode and a Hg/HgO reference electrode. The electrolyte is a solution of 6 M KOH. The voltage between the negative electrode and the reference electrode was defined as the discharge voltage. In every cycle, the alloy electrode was first charged at a constant current density, and following the resting for 15 min, it was discharged at the same current density to −0.500 V cut-off voltage. The environment temperature of the measurement was kept at 30 °C.

The electrochemical impedance spectra (EIS) and the Tafel polarization curves of the alloys were measured by an electrochemical workstation (PARSTAT 2273). The fresh electrodes were fully charged and then rested for 2 h up to the stabilization of the open circuit potential. The EIS spectra of the alloy electrodes were measured in the frequency range from 10 kHz to 5 mHz at 50% depth of discharge (DOD). The Tafel polarization curves were measured in the potential range of −1.2 to +1.0 V (vs. Hg/HgO) with a scan rate of 5 mV/s. For the potentiostatic discharge, the test electrodes in the fully charged state were discharged at 500 mV potential steps for 4500 s on electrochemical workstation (PARSTAT 2273), using the CorrWare electrochemistry corrosion software.

3. Results and discussion

3.1. Microstructure characteristics

The SEM images of the as-cast Cu_0 and $Cu_{0.4}$ alloys are illustrated in Fig. 1. It is quite evident that the as-cast alloys exhibit a typical dendritic structure. The substitution of Cu for Ni, instead of changing the morphology of the alloys, causes a significant refinement of the grains. The result obtained by energy dispersive spectrometry (EDS) reveals that the major phase of the as-cast alloys is Mg_2Ni phase (denoted by A). The $Cu_{0.4}$ alloy clearly exhibits some small massive particulates. The EDS analysis confirms that these particulates are Mg_2Cu phase (denoted by B).

The XRD profiles of the as-cast and quenched $Cu_{0.1}$ and $Cu_{0.4}$ alloys are depicted in Fig. 2. It is clear that all the as-cast and quenched alloys hold a single phase structure, visibly contrary with the result of the SEM observation as shown in Fig. 1. The absence of

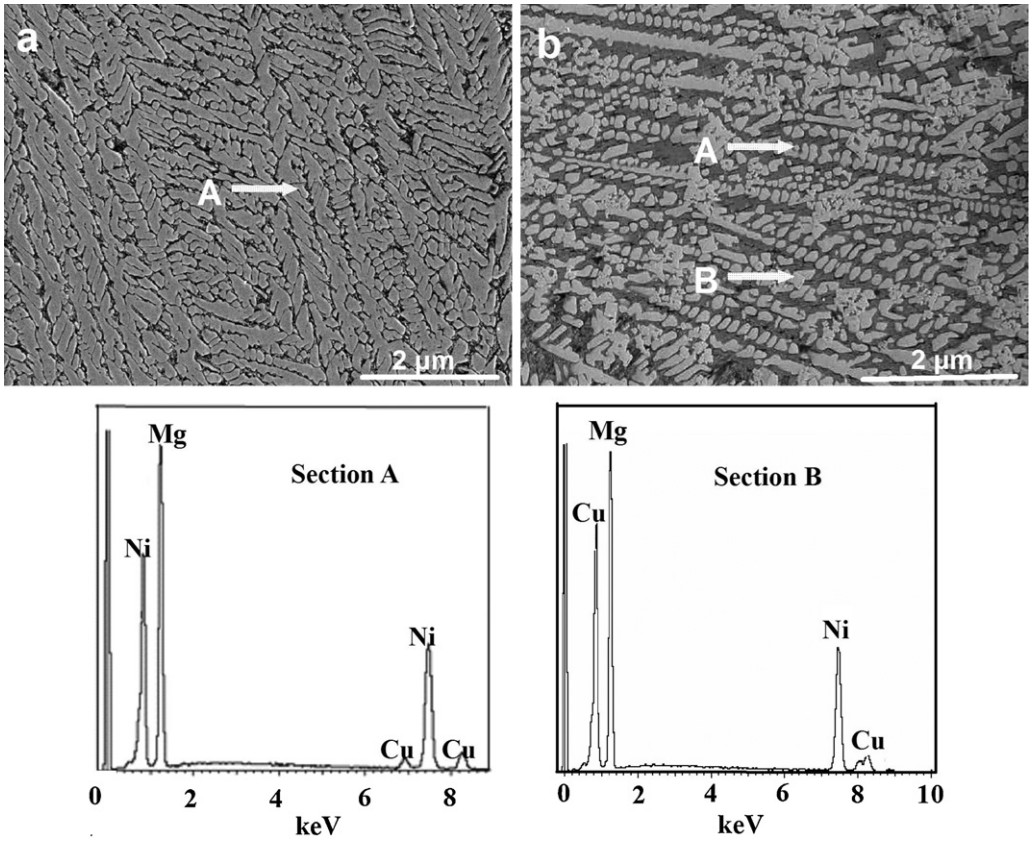

Fig. 1. SEM images of the as-cast alloys coupled with EDS spectra of sections A and B in (b): (a) Cu_0 alloy, (b) $Cu_{0.4}$ alloy.

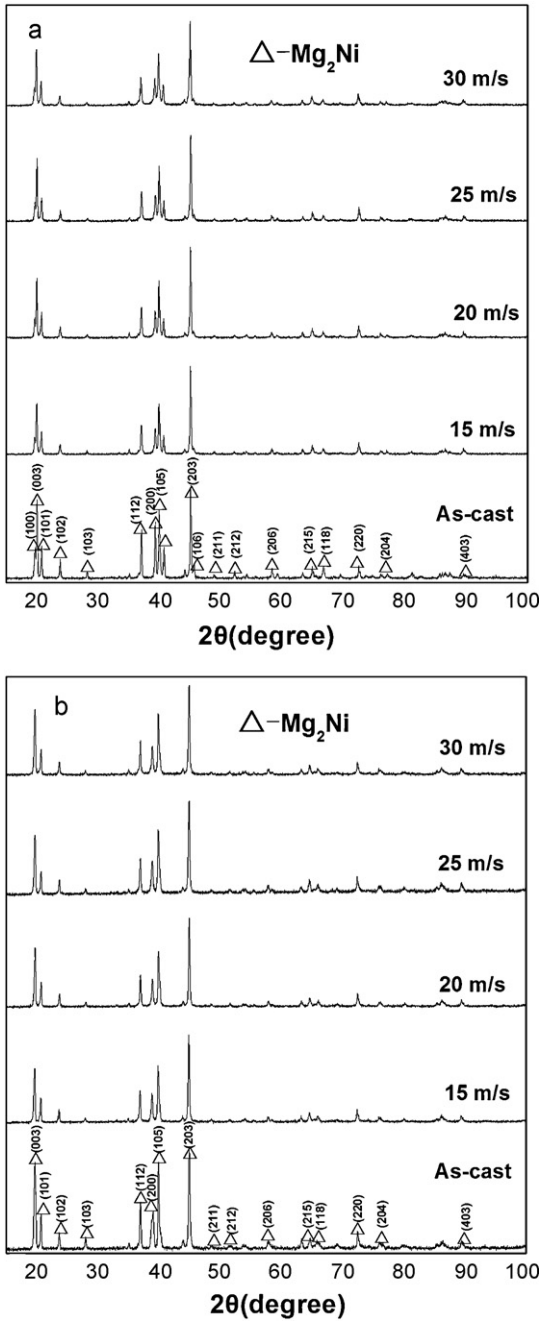

Fig. 2. XRD profiles of the as-cast and quenched alloys: (a) $Cu_{0.1}$ alloy, (b) $Cu_{0.4}$ alloy.

the diffraction peaks of the Mg_2Cu phase is probably due to its small amount and weak X-ray scattering intensity. The rapid quenching does not change the phase structure. Listed in Table 1 are the full width at half maximum (FWHM) values of the main diffraction peaks, the lattice parameters and the cell volumes of the of the $Cu_{0.1}$ and $Cu_{0.4}$ alloys, which were calculated by Jade 6.0 software. It can be derived from the Table 1 that the rapid quenching causes an evident increase in the FWHM values of the main diffraction peaks of the alloys and a visible enlargement in the lattice parameters and cell volumes of the alloys, which is doubtless attributed to the refined grain and the stored stress in the grains produced by the rapid quenching. Furthermore, the enlargement of the cell volume, caused by the Cu substitution, justifies the successful alloying of Cu with Mg_2Ni. Based on the FWHM values of the broad diffraction peak (2 0 3) in Fig. 2, the grain size $\langle D_{hkl}\rangle$ (nm) of the $Cu_{0.1}$ and $Cu_{0.4}$ alloy is calculated using Scherrer's equation, also listed in Table 1. It reveals that both the rapid quenching and the substitution of Cu for Ni cause a visible decline in the grain sizes of the alloys.

The HRTEM micrographs and electron diffraction patterns of the as-quenched $Cu_{0.4}$ alloys are illustrated in Fig. 3. It is clear that the crystalline structure of $Cu_{0.4}$ is independent of the quenching rate. Moreover, their electron diffraction (ED) patterns exhibit sharp multi-haloes, testifying the crystalline structure. HRTEM observations indicate that the as-quenched alloys are strongly disordered and nanostructured without the exhibition of any amorphous phase. This result well coincides with the XRD observation shown in Fig. 2.

3.2. Gaseous hydrogen absorption and desorption kinetics

The hydrogen absorption kinetics of the alloy is symbolized by the hydrogen absorption saturation ratio (R_t^a), which is a ratio of the hydrogen absorption capacity for a fixed time to the saturated hydrogen absorption capacity of the alloy, being calculated by formula, $R_t^a = C_t^a/C_{100}^a \times 100\%$, where C_{100}^a and C_t^a are hydrogen absorption capacities at 100 min and t min, respectively. The experimental result indicates that, for all the experimental alloys, the C_{100}^a values are more than 98% of their saturated hydrogen absorption capacities. Therefore, it is justifiable to take the C_{100}^a value as the saturated hydrogen absorption capacity of the alloy. Apparently, for a fixed time t, a larger saturation ratio R_t^a implies better hydrogen absorption kinetics. The evolution of the hydrogen absorption saturation ratio (R_5^a) ($t = 5$) of the alloys with the quenching rate is presented in Fig. 4. It reveals that the R_5^a values of the alloys notably increase with quenching rate rising. As the quenching rate is enhanced from 0 (as-cast is defined as with the quenching rate of 0 m/s) to 30 m/s, the R_5^a value grows from 53.5 to 93.6% for the $Co_{0.1}$ alloy, and from 57.7 to 91.4% for the $Co_{0.4}$ alloy. It is noteworthy that all the alloys exhibit similar R_5^a values at the quenching rate of 30 m/s, suggesting that the hydrogen absorption kinetics of the as-quenched alloy is strongly dependant upon its structure.

The hydrogen desorption kinetics of all the as-quenched nanocrystalline Mg_2Ni-type alloys are found to be superior to those of conventional polycrystalline materials with the same compo-

Table 1
Lattice parameters, cell volumes, FWHM values and grain sizes of the $Cu_{0.1}$ and $Cu_{0.4}$ alloys.

Quenching rate (m/s)	FWHM values		Grain sizes		Lattice parameters and cell volume					
	2θ (45.14°)		D_{203} (nm)		a (nm)		c (nm)		V (nm^3)	
	$Cu_{0.1}$	$Cu_{0.4}$	$Cu_{0.1}$	$Cu_{0.4}$	$Cu_{0.1}$	$Cu_{0.4}$	$Cu_{0.1}$	$Cu_{0.4}$	$Cu_{0.1}$	$Cu_{0.4}$
0	0.133	0.165	64	52	0.5210	0.5217	1.3252	1.3302	0.3115	0.3135
15	0.194	0.241	44	35	0.5212	0.5220	1.3259	1.3311	0.3119	0.3141
20	0.218	0.252	39	34	0.5215	0.5220	1.3262	1.3317	0.3124	0.3142
25	0.237	0.273	36	31	0.5216	0.5221	1.3277	1.3323	0.3128	0.3145
30	0.241	0.285	35	30	0.5216	0.5222	1.3303	1.3331	0.3134	0.3148

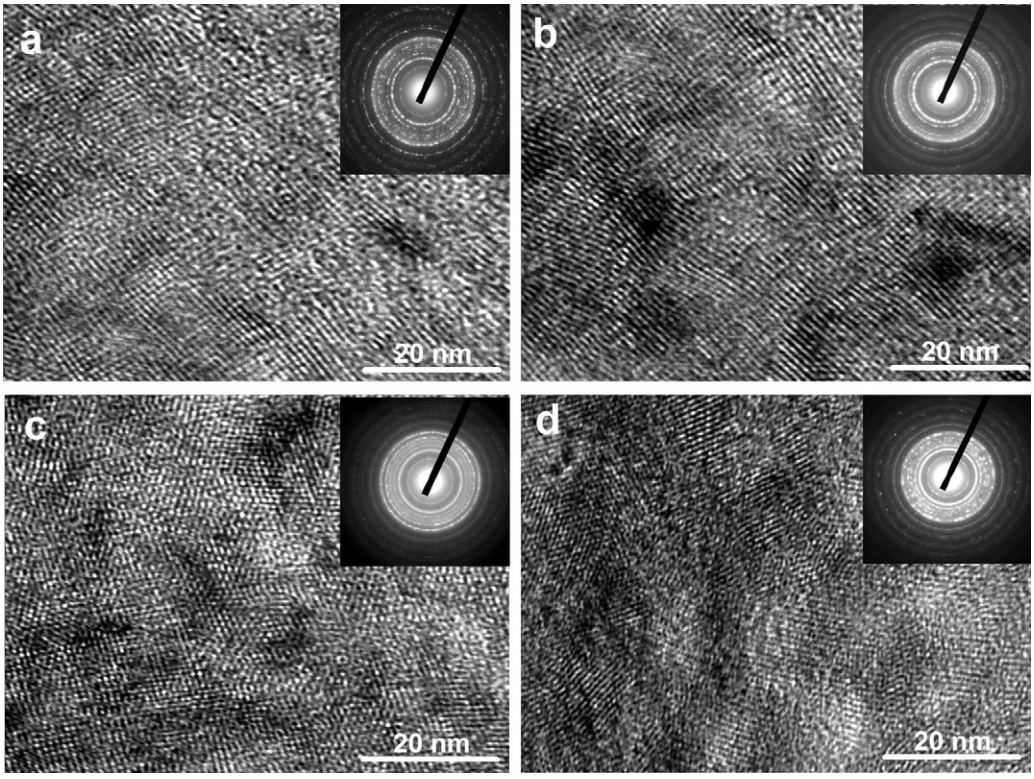

Fig. 3. HRTEM micrographs and ED of the as-quenched $Cu_{0.4}$ alloys: (a) 15 m/s, (b) 20 m/s, (c) 25 m/s, (d) 30 m/s.

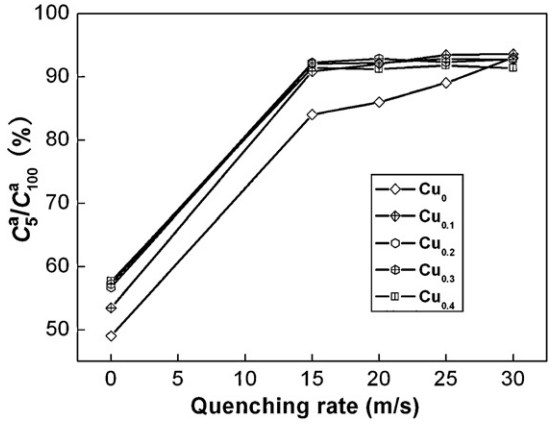

Fig. 4. Evolution of the hydrogen absorption saturation ratio (R_5^a) of the alloys with the quenching rate.

sition. This amelioration may be associated with the refinement of the grains produced by rapid quenching [13]. By refining the microstructure, a lot of new crystallites and grain boundaries are created which can act as fast diffusion paths for hydrogen absorption [14]. As the crystalline material undergoes the melt quenching, it becomes partially disordered and its structure transforms to nanocrystalline. Consequently, a high density of crystal defects such as dislocations, stacking faults and grain boundaries are introduced as shown in Fig. 5. The large number of interfaces and grain boundaries provide easy pathways for hydrogen diffusion and ultimately accelerates the hydrogen absorbing/desorbing process.

In order to identify the mechanism of the rapid quenching in ameliorating the hydrogen absorption kinetics of the alloy, the influence of the rapid quenching on the H diffusion ability in the alloy has been investigated. The H diffusion coefficients were measured by using the potential step method. A potential step of +500 mV versus the stabilized open circuit potential of the

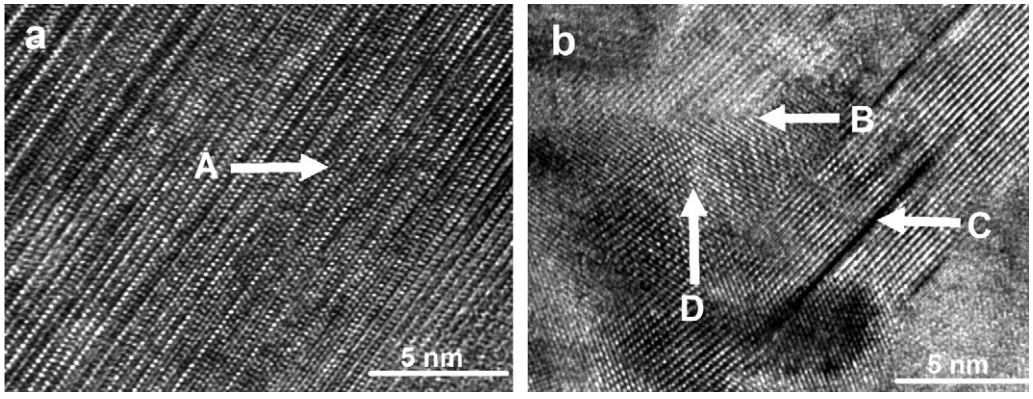

Fig. 5. The crystal defects in the as-quenched (30 m/s) $Cu_{0.4}$ alloy taken by HRTEM: (a) stacking fault denoted as A, (b) twin grain boundary denoted as B, dislocations denoted as C and sub-grain boundaries denoted as *D*.

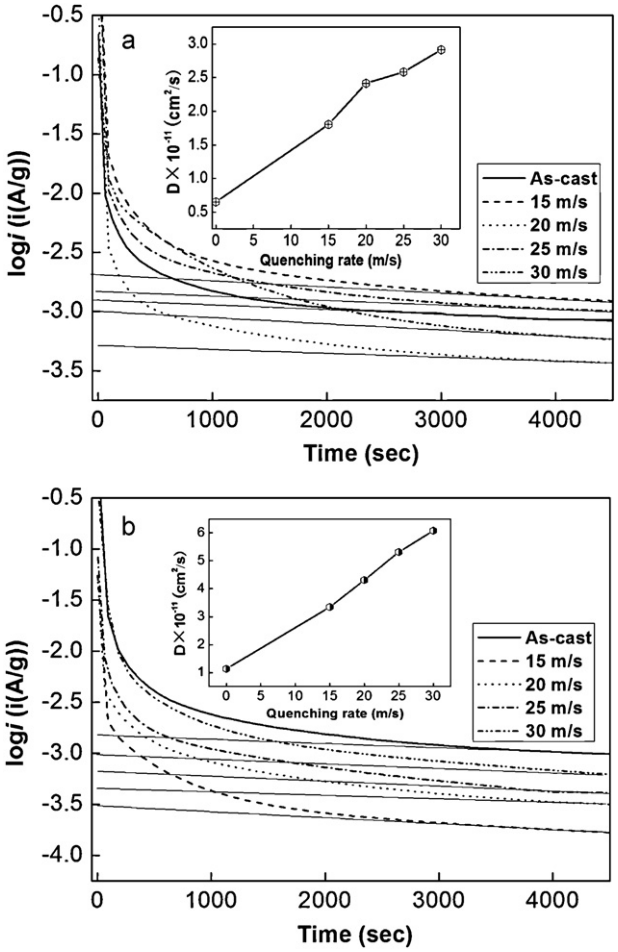

Fig. 6. Semilogarithmic curves of anodic current vs. time responses of the alloys: (a) $Cu_{0.1}$ alloy; (b) $Cu_{0.4}$ alloy.

fully charged electrode was applied and the decrease in discharge current as a function of time is monitored. Fig. 6 presents the semilogarithmic curves of anodic current versus working duration of the as-cast and quenched $Cu_{0.1}$ and $Cu_{0.4}$ alloys. The diffusion coefficient D of the hydrogen atoms in the bulk of the alloy can be calculated through the slope of the linear region of the corresponding plots according to following formulae [15].

$$\log i = \log\left(\pm\frac{6FD}{da^2}(C_0 - C_s)\right) - \frac{\pi^2}{2.303}\frac{D}{a^2}t \quad (1)$$

$$D = -\frac{2.303a^2}{\pi^2}\frac{d\ \log i}{dt} \quad (2)$$

where i is the diffusion current density (A/g), D is the hydrogen diffusion coefficient (cm^2/s), C_0 is the initial hydrogen concentration in the bulk of the alloy (mol/cm^3), C_s is the hydrogen concentration on the surface of the alloy particles (mol/cm^3), a is the alloy particle radius (cm), d is the density of the hydrogen storage alloy (g/cm^3), t is the discharge time (s), respectively. In Eq. (2), $(d \log i/dt)$ is the slope of the linear region of the semilogarithmic curves of anodic current versus working duration, which can easily be obtained by software origin 75. a is the alloy particle radius, supposing $a = 15\ \mu m$. Thus, hydrogen diffusion coefficient D can easily be obtained. The D values calculated by Eq. (2) are also shown in Fig. 6. It is viewable that an increase in the quenching rate brings about a notable rise in the D value. As the quenching rate rises from 0 to 30 m/s, the D value increases from 6.52×10^{-12} to $2.91 \times 10^{-11}\ cm^2/s$ for the $Cu_{0.1}$ alloy, and from 1.14×10^{-11} to $6.08 \times 10^{-11}\ cm^2/s$ for the $Cu_{0.4}$ alloy.

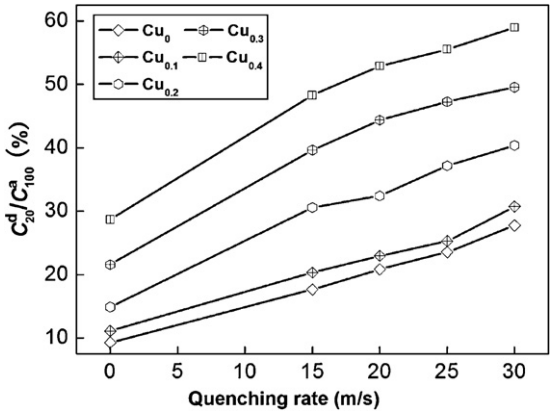

Fig. 7. Evolution of the hydrogen desorption ratio (R^d_{20}) of the alloys with the quenching rate.

Similarly, the hydrogen desorption kinetics of the alloy is indicated by the hydrogen desorption ratio (R^d_t), which is a ratio of the hydrogen desorption capacity for a fixed time to the saturated hydrogen absorption capacity of the alloy, being calculated by formula, $R^d_t = C^d_t/C^a_{100} \times 100\%$, where C^a_{100} is the hydrogen absorption capacity at 100 min and C^d_t is the hydrogen desorption capacity at t min, respectively. The hydrogen desorption ratio (R^d_{20}) ($t = 20$) of the alloys as a function of the quenching rate is depicted in Fig. 7. It reveals that the rapid quenching visibly enhances the R^d_{20} values of the alloys, suggesting that rapid quenching facilitates hydrogen desorption of Mg_2Ni-type alloy. With an increase in the quenching rate from 0 to 30 m/s, the R^d_{20} value grows from 11.1 to 30.7% for the $Cu_{0.1}$ alloy, and from 28.7 to 59.0% for the $Cu_{0.4}$ alloy. It has also been observed that the R^d_{20} value of the alloy markedly rises with an increase in the amount of Cu substitution at a fixed quenching rate. The hydriding/dehydriding kinetics of hydride materials depend on their chemical composition and crystalline structure [16]. The observed essential differences in the dehydriding kinetics of the quenched nanocrystalline Mg_2Ni type alloys may be associated with the different compositions of the alloys and their varying microstructures caused by the different quenching rates. It has already been reported that the high surface to volume ratios, i.e. high specific surface area, and the presence of large number of grain boundaries in nanocrystalline alloys facilitate the reaction of hydrogen desorption [17]. As reported by Zaluski et al. [18] and Orimo et al. [19], the hydriding/dehydriding characteristics at low temperatures (lower than 200 °C) of nanocrystalline Mg_2Ni alloys prepared by mechanical alloying can be improved by reducing the grain size (20–30 nm), due to hydrogen occupation in the disordered interface phase. Several reasons may be accounted for the enhancement in the hydrogen desorption kinetics of Mg_2Ni-type alloys caused by the substitution of Cu for Ni. Firstly, the partial substitution of element Cu for Ni in Mg_2Ni compound decreases the stability of the hydride and makes the desorption reaction easier [20]. Secondly, the presence of Mg_2Cu phase engenders a catalytic effect for the hydriding and dehydriding reactions of Mg and Mg-based alloys [21]. Furthermore, the addition of the third element Cu probably stabilizes the nanostructure of the alloy obtained by rapid quenching, which is very important for practical H-storage materials on the base of Mg_2Ni.

3.3. Electrochemical hydrogen storage kinetics

It is quite essential to inhibit the rapid attenuation in the discharge capacity even at a high charge/discharge current density for the practical application of hydride electrode in Ni-MH battery. Generally, the electrochemical kinetics of the alloy is

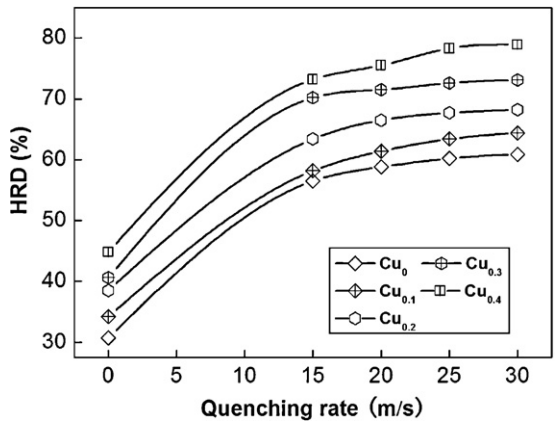

Fig. 8. Evolution of the high rate discharge ability (HRD) of the alloys with the quenching rate.

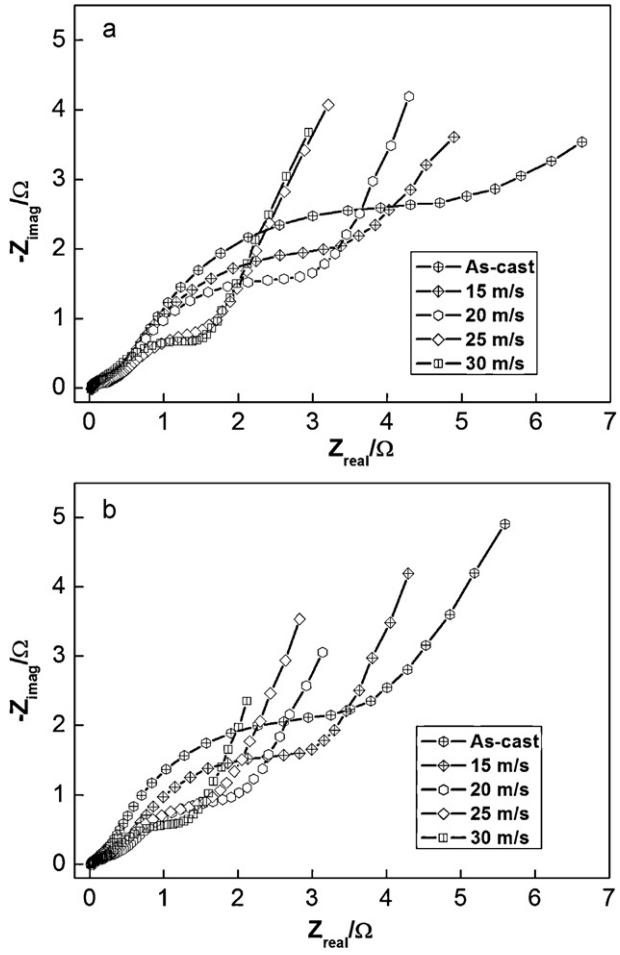

Fig. 9. Electrochemical impedance spectra (EIS) of the alloy electrodes at the 50% depth of discharge (DOD): (a) $Cu_{0.1}$ alloy, (b) $Cu_{0.4}$ alloy.

characterized by high rate discharge ability (HRD), being calculated by formula, $HRD = C_{100}/C_{20,max} \times 100\%$, where $C_{100,max}$ and $C_{20,max}$ are the maximum discharge capacities of the alloy electrode charged–discharged at the current densities of 100 and 20 mA/g, respectively.

The HRD values of the alloys as a function of the quenching rate are exhibited in Fig. 8. The HRD values of all the alloys grow with an increase in the quenching rate. As the quenching rate increases from 0 to 30 m/s, the HRD value rises from 34.2 to 64.4% for the $Cu_{0.1}$ alloy, and from 44.8 to 78.9% for the $Cu_{0.4}$ alloy. This enhancement in the HRD value of alloy may be attributed to the facilitation in the hydrogen diffusion caused by the rapid quenching (Fig. 6).

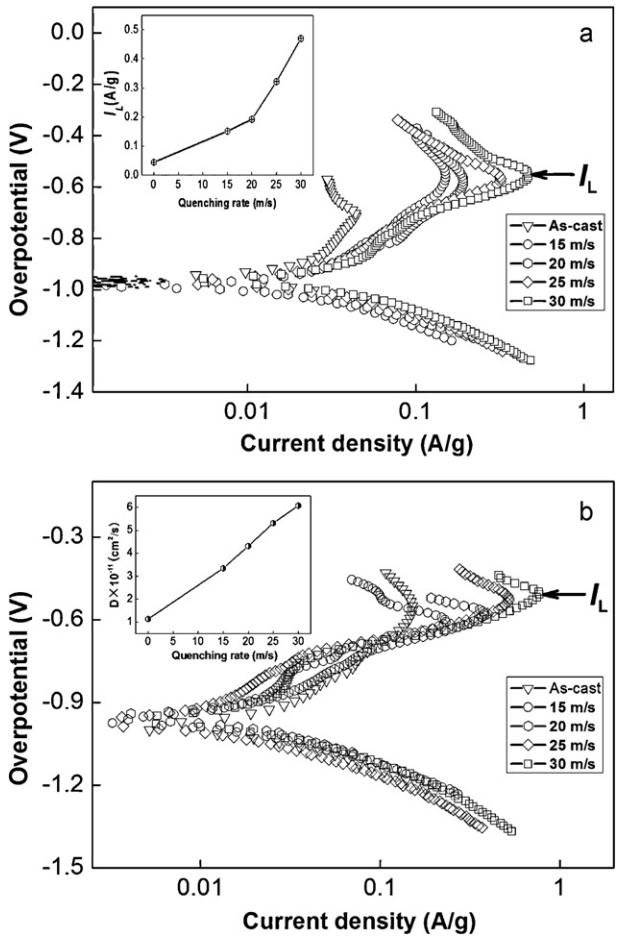

Fig. 10. Tafel polarization curves of the as-cast and quenched alloy electrodes at the 50% DOD: (a) $Cu_{0.1}$ alloy, (b) $Cu_{0.4}$ alloy.

High rate discharge ability is a kinetic performance of hydrogen absorbing/desorbing of the alloy electrode, basically depending on the charge transfer at the alloy–electrolyte interface and the hydrogen diffusion process from the interior of the bulk to the surface of alloy particle [22]. It is well known that the charge transfer at the alloy–electrolyte interface is characterized by the electrochemical reaction impedance on the surface of the alloy electrode, whereas the hydrogen diffusion ability from the interior of the bulk to the surface of alloy particle is described by the limiting current density. The electrochemical impedance spectra (EIS) of the as-cast and quenched $Cu_{0.1}$ and $Cu_{0.4}$ alloy electrodes at 50% DOD are illustrated in Fig. 9. It is viewable that each EIS spectrum consists of two semicircles followed by a straight line. As considered by Kuriyama et al. [23], the smaller semicircle in the high frequency region is attributed to the contact resistance between the alloy powder and the conductive material, while the larger semicircle in the low frequency region is accounted for the charge-transfer resistance on the alloy surface. The linear response at low frequencies is indicative of the hydrogen diffusion in the bulk alloy. Hence, the electrode kinetics of the as-cast and quenched alloys is determined by a mixed rate-determining process. It can be seen in Fig. 9 that the radius of the large semicircle in the low frequency for the $Cu_{0.1}$ and $Cu_{0.4}$ alloy clearly shrink with increasing quenching rate, implying that the refined grain by the rapid quenching facilitates charge-transfer of the alloy electrode.

Fig. 10 displays the Tafel polarization curves of the as-cast and quenched $Cu_{0.1}$ and $Cu_{0.4}$ alloy electrodes at the 50% DOD. It is visible that the anodic current densities first increase up to a limiting value and then decline sharply. The limiting current density, I_L, for each Tafel polarization curve indicates that an oxidation reaction takes place at the surface of the alloy electrode resulting in the generation of an oxidation layer at the surface of the alloy electrode that resists the further penetration of hydrogen atoms [24]. The decrease in the anodic charge current density with cycling implies that charging is becoming difficult. Therefore, the limiting current density, I_L, can be regarded as the critical passivation current density.

It is very evident in Fig. 10 that the I_L values of the alloys grow with the rise in the quenching rate. An increase in the quenching rate from 0 to 30 m/s yields the enhancement in the I_L value from 44.1 to 470.4 mA/g for the $Cu_{0.1}$ alloy, and from 148.5 to 480.2 mA/g for the $Cu_{0.4}$ alloy. Ratnakumar et al. [25] and Liu et al. [26] have shown that the variation in the limiting current can be governed by the solid state diffusion of hydrogen in metal-hydride electrode. Therefore, the positive impact of the rapid quenching on the I_L value may be ascribed to the variation in the structure of alloy induced by the rapid quenching.

4. Conclusions

The structures, gaseous and electrochemical hydrogen storage kinetics of the nanocrystalline $Mg_2Ni_{1-x}Cu_x$ (x = 0–0.4) alloys were investigated, and the conclusions obtained are summarized as follows:

All the as-quenched $Mg_2Ni_{1-x}Cu_x$ (x = 0, 0.1, 0.2, 0.3, 0.4) alloys hold an entire nanocrystalline structure and are free of amorphous phase. The rapid quenching renders an evident reduction in the grain size without altering the major phase Mg_2Ni in the alloy. Furthermore, the rapid quenching itself significantly improves the gaseous and electrochemical hydrogen storage kinetics of the alloys. The hydrogen absorption saturation ratio (R_5^a) and the hydrogen desorption ratio (R_{20}^d) as well as the high rate discharge ability all increase with rising quenching rate. As the quenching rate grows from 0 to 30 m/s, the R_5^a, R_{20}^d, and HRD values of the $Cu_{0.4}$ alloy increase from 57.7%, 28.7% and 44.8% to 91.4%, 59.0% and 78.9% respectively.

Acknowledgements

This work is supported by National Natural Science Foundations of China (50871050 and 50961009), Natural Science Foundation of Inner Mongolia, China (2010ZD05) and Higher Education Science Research Project of Inner Mongolia, China (NJzy08071).

References

[1] I.P. Jain, C. Lal, A. Jain, Int. J. Hydrogen Energy 35 (2010) 5133–5144.
[2] X.Y. Zhao, L.Q. Ma, Int. J. Hydrogen Energy 34 (2009) 4788–4796.
[3] S.N. Kwon, S.H. Baek, D.R. Mumm, S.H. Hong, M.Y. Song, Int. J. Hydrogen Energy 33 (2008) 4586–4592.
[4] T. Spassov, P. Delchev, P. Madjarov, M. Spassova, Ts. Himitliiska, J. Alloys Compd. 495 (2010) 149–153.
[5] P. Palade, S. Sartori, A. Maddalena, G. Principi, S. Lo Russo, M. Lazarescu, G. Schinteie, V. Kuncser, G. Filoti, J. Alloys Compd. 415 (2006) 170–176.
[6] Y. Wu, M.V. Lototsky, J.K. Solberg, V.A. Yartys, W. Han, S.X. Zhou, J. Alloys Compd. 477 (2009) 262–266.
[7] S. Kalinichenka, L. Röntzsch, T. Riedl, T. Gemming, T. Weißgärber, B. Kieback, Int. J. Hydrogen Energy 36 (2011) 1592–1600.
[8] Á. Révész, Zs. Kánya, T. Verebélyi, P.J. Szabó, A.P. Zhilyaev, T. Spassov, J. Alloys Compd. 504 (2010) 83–88.
[9] J. Lang, J. Huot, J. Alloys Compd. 509 (2011) L18–L22.
[10] Y.H. Zhang, B.W. Li, H.P. Ren, X.X. Ding, X.G. Liu, L.L. Chen, J. Alloys Compd. 509 (2011) 2808–2814.
[11] Y.H. Zhang, D.L. Zhao, B.W. Li, H.P. Ren, S.H. Guo, X.L. Wang, J. Alloys Compd. 491 (2010) 589–594.
[12] G.K. Williamson, W.H. Hall, Acta Metall. 1 (1953) 22–31.
[13] K. Tanaka, Y. Kanda, M. Furuhashi, K. Saito, K. Kuroda, H. Saka, J. Alloys Compd. 293–295 (1999) 521–525.
[14] Y. Wu, W. Han, S.X. Zhou, M.V. Lototsky, J.K. Solberg, V.A. Yartys, J. Alloys Compd. 466 (2008) 176–181.
[15] G. Zhang, B.N. Popov, R.E. White, J. Electrochem. Soc. 142 (1995) 2695–2698.
[16] G. Mulas, L. Schiffini, G. Cocco, J. Mater. Res. 19 (2004) 3279–3289.
[17] T. Spassov, U. Köster, J. Alloys Compd. 279 (1998) 279–286.
[18] L. Zaluski, A. Zaluska, J.O. Ström-Olsen, J. Alloys Compd. 253–254 (1997) 70–79.
[19] S. Orimo, H. Fujii, K. Ikeda, Acta Mater. 45 (1997) 331–341.
[20] J.H. Woo, K.S. Lee, J. Electrochem. Soc. 146 (1999) 819–823.
[21] M.Y. Song, S.N. Kwon, J.S. Bae, S.H. Hong, Int. J. Hydrogen Energy 33 (2008) 1711–1718.
[22] A. Gasiorowski, W. Iwasieczko, D. Skoryna, H. Drulis, M. Jurczyk, J. Alloys Compd. 364 (2004) 283–288.
[23] N. Kuriyama, T. Sakai, H. Miyamura, I. Uehara, H. Ishikawa, T. Iwasaki, J. Alloys Compd. 202 (1993) 183–197.
[24] X.Y. Zhao, Y. Ding, L.Q. Ma, L.Y. Wang, M. Yang, X.D. Shen, Int. J. Hydrogen Energy 33 (2008) 6727–6733.
[25] B.V. Ratnakumar, C. Witham Jr., R.C. Bowman, A. Hightower, B. Fultz, J. Electrochem. Soc. 143 (1996) 2578–2584.
[26] Y.F. Liu, H.G. Pan, M.X. Gao, Y.F. Zhu, Y.Q. Lei, Q.D. Wang, Int. J. Hydrogen Energy 29 (2004) 297–305.